Combination of two Fabry-Pérot etalons and a grating spectrograph for imaging polarimetry of the Sun

Lucia Kleint[a,c], Alex Feller[b] and Michele Bianda[c,a]

[a]Institute of Astronomy, ETH Zurich, CH-8092 Zurich, Switzerland
[b]Max-Planck-Institut für Sonnensystemforschung, D-37191 Katlenburg-Lindau, Germany
[c]Istituto Ricerche Solari Locarno, Via Patocchi, CH-6605 Locarno Monti, Switzerland

ABSTRACT

Imaging spectroscopy of the Sun is a challenging task usually performed with Fabry-Pérot etalons. The common setup is a combination of two or three etalons in series and a narrow-band prefilter. The requirement of one, usually expensive prefilter for every desired wavelength limits the number of spectral regions that can be observed.

We present a novel instrument combination consisting of two Fabry-Pérot etalons and a grating spectrograph, which allows for observations in any wavelength between 390 nm and 660 nm without the need for narrow-band prefilters. Furthermore, two or more adjacent monochromatic images are projected on the detector, each image corresponding to a different spectral transmission peak of the Fabry-Pérot filtergraph. Together with our Zurich Imaging Polarimeter (ZIMPOL) the system is installed at the telescope of the Istituto Ricerche Solari Locarno (IRSOL) where it will be used for two-dimensional spectropolarimetry. We present a description of the instrument and test observations.

Keywords: instrumentation, Fabry-Pérot interferometer, spectrograph - spectropolarimetry - Sun

1. INTRODUCTION

For over 30 years, Fabry-Pérot (FP) interferometers have been widely used for spectroscopic observations of the Sun. Though many different instrument layouts exist there is one commonality in all the setups: A filter with a narrow passband is used to select one of the periodically repeating transmission peaks of the FP interferometers, thus giving monochromatic images. The main difference in all setups is the type of prefilter and the number of FP etalons. A combination of several FP interferometers in series offers the advantage of an increase of the free spectral range (FSR), i.e. the distance between two successive transmission peaks.[1] The prefilter has to be chosen to have a passband width of less than the FSR to avoid parasitic light from other wavelengths than the desired one. The most common choice for such prefilters are narrow-band interference filters with a typical FWHM of less than half a nanometer.[2,3] The obvious disadvantage is that one dedicated prefilter is required for every desired spectral region. Combined with the fact that narrow-band filters are expensive, other solutions have been sought.

One possibility which was used in the past is a universal birefringent filter (UBF) in combination with a FP.[4,5] This setup allowed to observe any wavelength between 4200 and 7000 Å with a spectral resolving power of about 300'000 and a seeing-limited spatial resolution. A problem for this system is that both passbands have a periodical transmission, the one of the UBF resembling a sinc^2-function and the FP passband being described by an Airy function. Therefore, this system required a very careful tuning to eliminate parasitic light. Another disadvantage is the low transmission of the UBF ranging from 4 to 9 %. While there were enough photons for spectroscopy, high-precision polarimetry would probably be impossible with such a system.

Another setup was used at the Arcetri Solar Tower: A combination of one FP etalon and a grating spectrograph.[6] While their wavelength range was limited to 5500 - 6500 Å due to the coating of the etalon, they achieved a very high spectral resolution of 900'000 (at 6328 Å). This setup was used with a photomultiplier and therefore did not have any spatial resolution.

Our goal is to combine several advantages of the previously mentioned systems into one. We use two Y-cut $LiNbO_3$ FP etalons in series which results in a FSR of about 5 Å (wavelength dependent). They can be tuned to any wavelength between 3900 and 6600 Å. The high-resolution Czerny-Turner spectrograph of IRSOL is used

Ground-based and Airborne Instrumentation for Astronomy II, edited by Ian S. McLean, Mark M. Casali,
Proc. of SPIE Vol. 7014, 701414, (2008) · 0277-786X/08/$18 · doi: 10.1117/12.787923

to choose one distinct wavelength. By replacing the spectrograph slit with a field stop we get two-dimensional images on the camera. Combined with ZIMPOL we have a two-dimensional spectropolarimeter with a possible, photon-limited accuracy of better than 10^{-4}. The main advantage compared to other FP systems is the ability to observe any desired wavelength within the aforementioned spectral range without the need of an expensive collection of custom-made narrow-band filters (FWHM $<$ 5 Å). Instead, we use our already available order-sorting filters with a much larger FWHM of order 200 Å. Our comparatively small telescope, the moderate seeing conditions on one side, the photon limited polarimetric accuracy of ZIMPOL on the other side bring about scientific objectives that differ from the objectives followed by most current solar telescopes. We do not aim for maximum spatial resolution but for high polarimetric accuracy and a very high spectral resolution.

We plan to employ our system for synoptic observations in several lines, searching for spatial variations of the Hanle and Zeeman effects. Imaging of the Hanle effect will open new possibilities to study the structure and distribution of weak, directed or turbulent magnetic fields in the solar atmosphere, as well as their evolution with the solar cycle. First images have been obtained by Stenflo et al. (2002)[7] using the UBF with a band width of 0.2 Å, but the advantage of our instrument is a much narrower passband. Also, statistical analyses, of sunspots for example, may allow us to derive a detailed height dependence of the magnetic fields by observing many different lines. If only one of the etalons is used, simultaneous images of many spectral points in a line can be taken. Such a setup overcomes the disadvantage of other systems that have to tune through the wavelengths thus not getting exactly simultaneous images. Applications include immediate imaging of flares, differential Hanle effect measurements, especially in molecular bands where the many spectral windows can sample different lines, and the derivation of the temperature structure and its depth dependence by observing broad chromospheric lines.

2. INSTRUMENTATION

Our motivation was to create an instrument combination that would allow high-precision spectropolarimetry in any desired wavelength in the range of 390 - 660 nm. Using the already existing good infrastructure of our telescope including a high-resolution spectrograph we were able to set up the new instrument combination with minimal changes. In the following sections we will present the main components of our current setup.

2.1 Telescope and spectrograph

The IRSOL telescope is an evacuated Gregory Coudé instrument with an aperture of 45 cm and an effective focal length of 25 m. This type of telescope has an instrumental polarization that depends only on the declination of the Sun and therefore, is practically constant during one observing day which greatly facilitates the polarization compensation or a subsequent correction. At the equinoctes the instrumental polarization vanishes completely.[8] Since 1990, the instrument is equipped with a high resolution Czerny-Turner spectrograph with a 180 $\times$ 360 mm grating with 316 lines/mm and a blaze angle of 63.5°.

The setup is shown in Fig. 1. The image is not to scale and two folding mirrors after the FP etalons are left out. The light from the telescope exit window first passes through polarimetric calibration optics (CO). Through their placement right after the telescope exit, all instrumental effects of the optical elements situated later in the beam can be calibrated. Next, there is the polarization compensation plate (CP) and the modulator package (MP) that are described in Section 2.3. A derotator (DEROT) compensates for image rotation and an interference filter (IF) selects the desired order of the spectrograph before the light gets deflected to the basement. The primary focus is located after the interference filter. Mirror CM1 collimates the beam and both FP etalons (FPE) are situated close to the pupil image. Mirror IM1 creates a focus where a field stop (FS) selects the final field of view. A second collimating mirror (CM2) sends the light to the spectrograph grating (G). After the grating, mirror IM2 focusses the spectrum onto the ZIMPOL camera (CAM).

2.2 Fabry-Pérot etalons

2.2.1 Etalon control

Unlike air-spaced etalons which are tuned by varying the distance between the two reflecting plates, lithium niobate etalons can be tuned by varying their optical thickness, either through temperature changes (thermal expansion and temperature dependence of the refractive index) or by varying the applied voltage (piezo effect

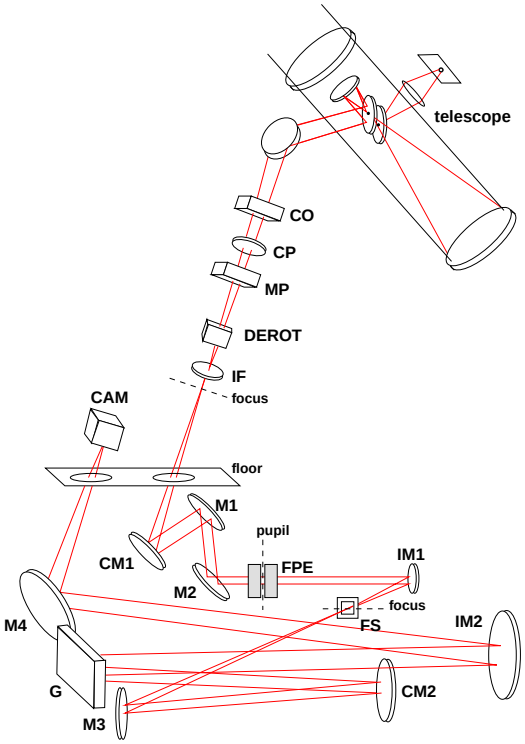

Figure 1. The setup for the FP spectrograph instrument combination at IRSOL. Generally, plane mirrors are denoted by M, collimating mirrors by CM and imaging mirrors by IM. See text for an explanation of all labels.

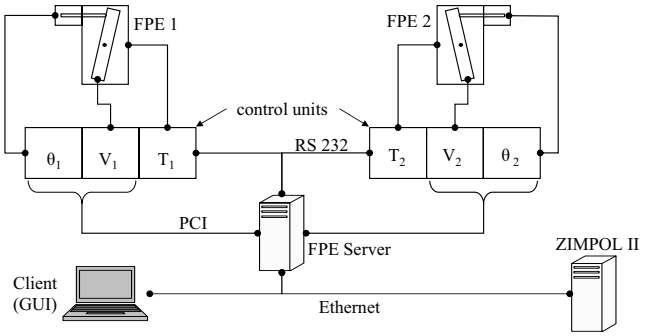

Figure 2. FP control (from Feller, 2008). The tilt, the voltage and the temperature of the etalons can be set via user interface.

and electro-optic effect). We use the slow thermal tuning to set the etalons to a home position, for example such that at 0 V the passbands of both etalons coincide with the desired line center. To scan through a line profile the much faster voltage tuning is used while the etalon is kept at a fixed temperature with a precision of $\pm$ 0.02 °C. The calibration and tuning process is described in section 3.

Fig. 2 outlines the etalon control. Two separate control units, operated by the FP server, set the temperature, the voltage and the tilt angle of the individual etalons. The FP server is connected to the ZIMPOL system and all etalon-specific commands can be set directly in a user interface that also controls all other ZIMPOL components.

2.2.2 Etalon-spectrograph combination

The principles of the different setups can be seen in Fig. 3. Below the horizontal line, the passbands of a FP interferometer and a narrow-band prefilter are shown with both maximum transmissions scaled to unity. The passband of the prefilter (dashed) is centered around a wavelength λ_n and selects one of the periodically repeating transmission peaks of the FP (solid). The FP etalon can be tuned to any wavelength, in the example one peak is also centered at λ_n. Therefore, only this wavelength passes through the whole system, giving a monochromatic image on the camera. This is the most common setup used at ground-based solar telescopes. We have used this type of setup both at IRSOL and at the Swedish Solar Telescope on La Palma.[9]

Above the solid line our new system is outlined. Top left is the passband of an interference filter with a typical FWHM around 200 Å. Below, the passband of a FP system is shown, note the different spacings in wavelength ($\lambda_{n+1} - \lambda_n$ are the same in both pictures). Our FP have a FSR of about 5 Å when they are used in tandem. Without a spectrograph, a camera would image a mixture of different wavelengths given by the sum of all transmission peaks in the range of the interference filter. By using a spectrograph one can select one of the FP transmission peaks and get a monochromatic image on the camera.

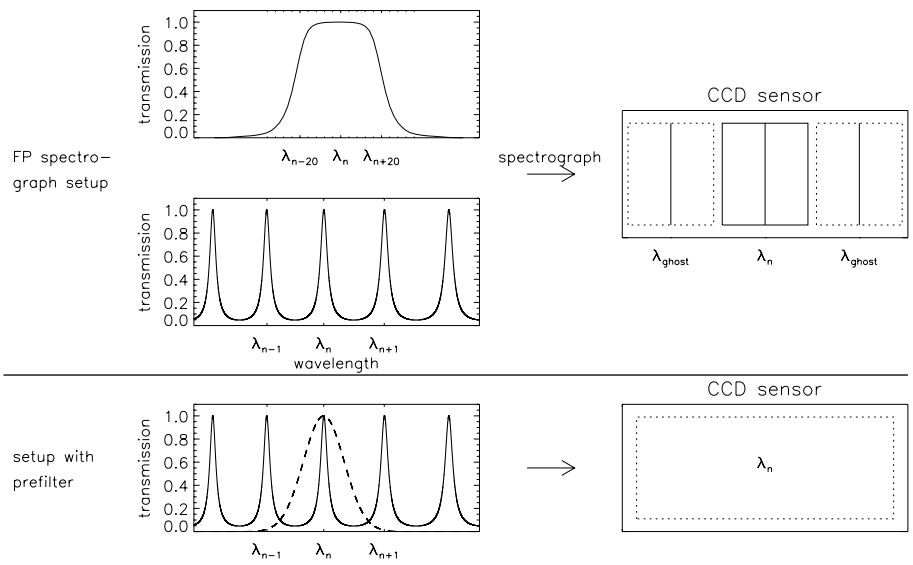

Figure 3. Bottom: Schematic drawing of the passbands of the common system - FP (solid line) and prefilter (dashed line) - and a monochromatic image on the camera. Top: The passbands of our new system (interference filter and FP) that, combined with the spectrograph passband, result in several monochromatic images on the camera.

2.2.3 Ghost images

In reality, a transmission spectrum of two etalons does not look as simple as the plot on the left but there are several smaller transmission peaks coming from reflections between the two etalons. We can get rid of most of these ghost images by slightly tilting the second etalon (0.1°). Ghost images also occur if passbands with a finite width overlap which is the case for our two etalons and cannot be changed since these parameters depend on the given FSR of the etalons and the FWHM of the transmission peaks. Two of these ghost peaks are situated close to the central wavelength λ_n ($\pm$ 1.7 Å distance when looking at the 4607 Å line) and give fainter adjacent images on the camera. Using a slit in front of the spectrograph would give three vertical lines (solid vertical lines, top right image) at λ_n and the two ghost wavelengths. By replacing the slit with a field stop the images get two-dimensional while the middle image (thick rectangle) has the maximum intensity though that could by changed through a detuning of the FP. The maximum size of the field stop is limited by the fact that the images should not overlap on the CCD sensor. Another possibility would be to use only one of both FP etalons for this setup. The FSR would then be smaller and there would be a lot more spectral windows on the camera (very dependent on the wavelength, for example 11 adjacent images for FP 1 or 8 for FP 2 at λ=4607 Å).

2.2.4 Spectral characteristics

The collimated FP setup induces a small (15 mÅ) radial blueshift of the passband across the field of view (FOV). With respect to the center of the FOV the wavelengths of all other points get shifted to the red. This shift can be measured and corrected for during data reduction. To avoid strong ghost images coming from reflections between the two FP etalons, FP 2 is tilted by 0.1°. This leads to a small phase error between the individual etalons which increases linearly across the FOV up to a maximum value of 2.5 mÅ. Table 1 gives a short overview of the main FP characteristics. The temperature and voltage characteristics are compiled from different calibration measurements which lie about half a year apart. The first values are derived from an actual measurement, the values in parentheses are taken from Feller (2008).[9] The data suggest a slight longterm variability of these parameters. This will be monitored in the future and more frequent calibrations will be performed.

Table 1. Main characteristics of our FP system.

Type	$LiNbO_3$ Y-cut, made by CSIRO	
Aperture	60 mm (40 mm used in our setup)	
Cavity thickness	0.985 mm ± 0.6 nm	0.757 mm ± 0.5 nm
Wavelength range	390 - 660 nm	
Reflectivity	0.925	

Performance examples at 4607 Å for the extraordinary axis

effective finesse	10 - 40	
avg. FSR of the tandem	5.3 Å	
avg. FSR of each etalon	416 (414) mÅ	540 (538) mÅ
Temperature response	∼165 (169) mÅ/°C	∼140 (136) mÅ/°C
Voltage response	79 (76) mÅ/kV	96 (102) mÅ/kV
Radial wavelength shift across FOV	15 - 25 mÅ	

2.3 Zurich imaging polarimeter

For our measurements we use the established Zurich Imaging POLarimeter II (ZIMPOL) system.[10,11] It basically consists of a photo-elastic modulator (PEM) which periodically modulates the polarization of the incoming light, a polarizer which converts the polarisation modulation into an intensity modulation and a demodulating camera with a special, masked sensor. In the following a short description will be presented, mainly of parts that have changed or were improved since the description of Gandorfer et al. (2004).[10]

The polarization-calibration optics consist of a Glan-Thompson polarizer and an achromatic quarter-wave plate. These motorized and remotely controlled components can be inserted into the beam and rotated to create any elliptic polarization state. The achromatic Quartz and MgF_2 retardation plate is easily exchangeable when different wavelengths are observed and our models cover the range from 300 - 470 nm and 460 - 680 nm.

As the influence of detector nonlinearities and calibration errors scale with the polarization offset, a glass plate is used to compensate for the linear polarization produced by the telescope.[12] The glass plate is tilted and rotated with respect to the optical axis so that it produces a linear polarization state which is opposite to and therefore cancels with the telescope polarization. An automatic procedure measures the linear polarization and its direction and orients the plate to compensate up to the level of 10^{-4}.

The PEM has a basic mechanical vibration frequency of 42 kHz, well above the frequency spectrum of atmospheric turbulences in the range of several 100 Hz. This gives the great advantage of no seeing-induced cross-talk because of this very fast modulation. In our setup, the circular polarization is modulated with the mechanical vibration frequency while one component of the linear polarization is modulated with the double of this frequency. A dielectric beam-splitter with 40 × 40 mm aperture is mounted to the PEM and transforms the generated polarization modulation into an intensity modulation that can be imaged by a camera.

After its path through the FP system and the spectrograph, the light passes through telecentric reduction optics and falls onto the ZIMPOL camera. The selfmade ZIMPOL camera has a custom-made CCD55-20 from E2V with 770 × 576 pixels (pixel size 22.5 μm × 22.5 μm). The CCD chip has an open electrode structure leading to an increased sensitivity in the UV. Because of the special ZIMPOL characteristic of polarisation demodulation by charge shifting, three out of every four pixel rows are covered by a mask.[10] This vertical charge-shifting occurs simultaneously with the modulation giving a simultaneous image of different polarization states. The frame is read out after many modulation cycles. Therefore, only 576/4 = 144 pixels are used for the actual vertical resolution while the masked pixels serve as temporary buffers. The implementation of microlenses, which the former versions of ZIMPOL did not have, leads to a great improvement in light gathering power since the light that would be lost at the masked rows is now directed to the unmasked rows. A cylindrical array of microlenses

with a focal length of 150 μm was actively aligned and mounted to the housing of the CCD chip, leaving a 150 μm wide air gap between the microlenses and the chip. The focal length was chosen to be as short as possible to minimize the angle dependency of the incoming light and to achieve the smallest possible light spot diameter on the pixels. The sensitivity is enhanced by a factor of 3 (red) to 6 (blue) compared to the camera without microlenses.[13] The large increase in UV sensitivity results from the precise direction of the light through the open electrode structure.

3. TUNING AND CALIBRATIONS OF THE FP

There are two types of spectral calibrations for our FP system: (1) A long-term calibration that is performed once for every desired spectral window (few Å wide) and that has the purpose of determining the temperature and voltage dependence of both etalons. (2) A much faster daily calibration that has the purpose of eliminating small tuning errors. The voltage and temperature dependence are non-linear and impossible to model over the whole FP working range, which is why a separate calibration is necessary for every spectral window.

First, a solar reference spectrum is taken with both etalons out of the beam and fitted to an atlas for an exact wavelength calibration. At the longterm calibration transmission spectra of both FP etalons are recorded using the spectrograph at (at least) three different temperatures and at different voltages and a simplified model of the etalon transmission

$$T = \frac{p_0}{1 + p_1 \sin\left(p_2(\lambda - p_4)\right)^2} + p_3 \tag{1}$$

fitted to the data with five free parameters $p_0, \ldots, p_4$.[9] Based on the result of this procedure a fixed temperature is chosen by the user, depending on the desired spectral home position of the FP. Usually, a wavelength close to center of the observed line is chosen and the passband of both FP etalons is centered at this wavelength at 0 V.

For the daily calibration a scan through the whole voltage range is performed for each individual etalon (at the temperature that was determined from the long term calibration). An IDL routine automatically determines and fits the positions of the passbands of each FP and writes a parameter file containing the fit parameters. This file is read into the ZIMPOL system and a simple function converts the wavelength into two values for the voltages synchronizing both FP etalons. Fig. 4 illustrates the daily calibration process.

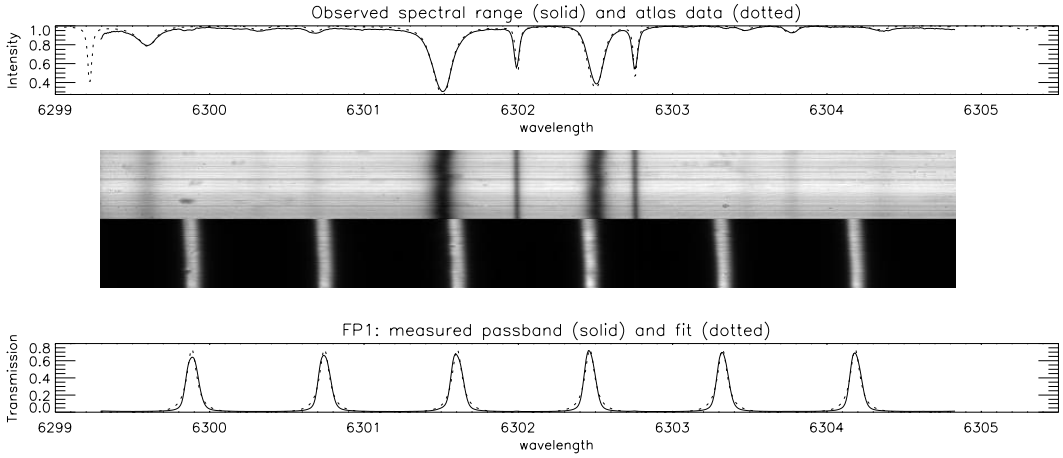

Figure 4. Top: Sample reference image and its average along the slit (solid) showing the region around the Fe 6301.5 and 6302.5 lines. The dotted line is the spectrum from the FTS atlas for comparison. The fit gives the exact wavelength step per pixel and the observed wavelength range. The bottom image shows the passbands of FP1 (solid) at 0 V, averaged along the slit in the bottom plot. The model transmission fit is shown as dotted line and helps to determine the center of the passband precisely.

Theoretically, the daily calibration can be used independently of the long-term calibration. In this case the 0 V position of the individual etalons is arbitrary but observations are possible even though the etalons are not

operating at their optimum temperature setting points. The longterm calibration is however indispensable if observations without the spectrograph and with a narrowband prefilter are performed.

Fig. 5 shows the - in a small wavelength range - linear dependence of the wavelength vs. voltage. These plots are the result of the whole calibration routine and the fits (solid lines) are used for the calculation of wavelength into voltage for the FP etalons.

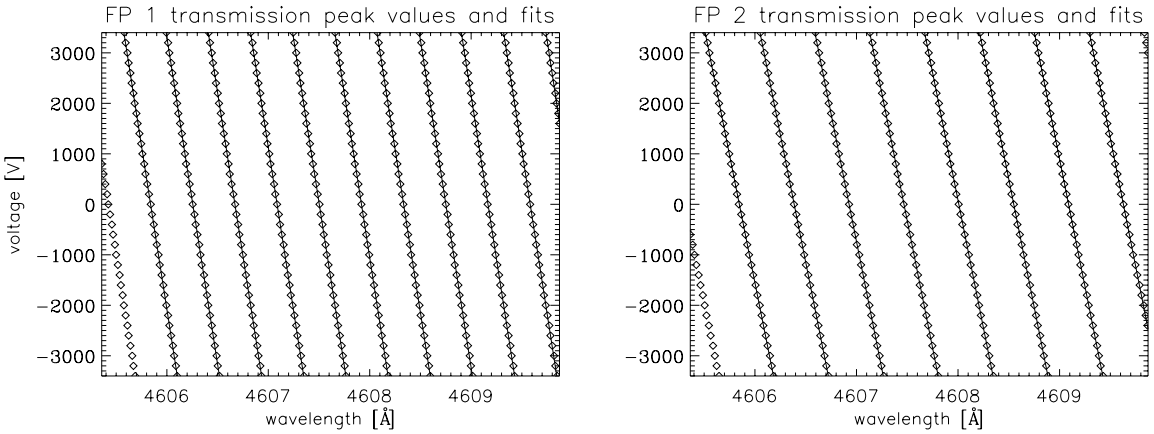

Figure 5. Measurements of the voltage - wavelength dependence of the transmission maxima of the passband for FP1 (left) and FP2 (right). The solid lines show the linear fits through the data points to interpolate missing wavelengths.

The measured FWHM of the etalon passbands is significantly larger than the value stated by the manufacturer. We have not found out the exact reason yet. An improvement of the FWHM can be achieved if we stop down the etalon apertures, but this has the obvious disadvantage of less photons. The passband broadening is likely the result of cavity thickness errors. Therefore, we plan to measure thickness maps of the etalons.

4. EXAMPLES OF DATA

We have successfully tested the FP spectrograph system with observations of the Sr 4607 Å line, Fe 6302.5 Å and Fe 6301.5 Å lines and H-α 6563 Å line. A scan through the lines shows the variable intensity. We plan to start polarimetric observations in the summer and here we only present a preliminary example of our test scans.

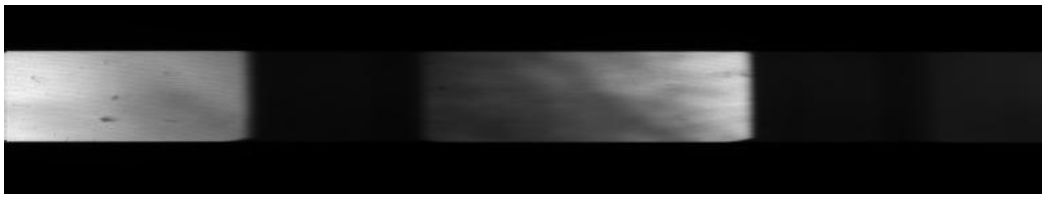

Figure 6. Sample image of H-α showing an image with the wavelength 6563.3 Å in the middle and two adjacent ghost images at 6563.3 $\pm$ 3.74 Å

Fig. 6 shows a sample image of a plage region on May 14, 2008. The H-α line core (middle) and two adjacent ghost images are visible. The left ghost image clearly does not show as many structures as the line core and the right ghost image is very faint. The reason for the image limitation in vertical direction is a non-ideal field stop which will be exchanged in the future.

An image of the USAF target is shown in Fig. 7. It is used to determine the astigmatism and the resolution.

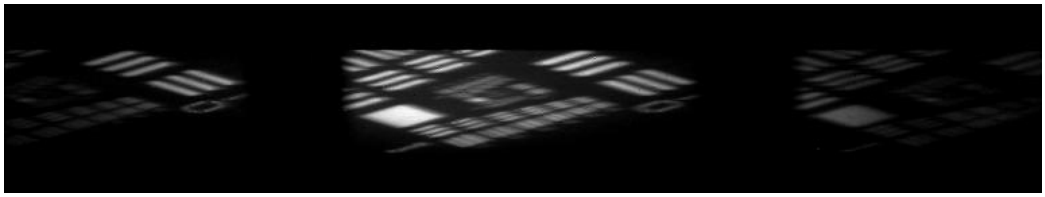

Figure 7. USAF target image (taken at wavelengths 4607.3 ± 1.7 Å)

5. CONCLUSION AND OUTLOOK

In the following, we will summarize some advantages and some disadvantages of our system.

Advantages

- The main advantage is the ability to observe any line in our working range (390 - 660 nm) with a calibration that only takes 20 minutes per line.
- We de not require any expensive narrow-band prefilters.
- Photon-limited spectropolarimetry is possible with adequate spatial resolution.

Disadvantages

- The FOV is limited by the ghost images next to the desired image. One can however leverage this constraint in certain wavelength regions by making use of the ghosts to obtain images in more than one wavelength simultaneously.
- The camera and the setup are not very sensitive in the blue wavelength range and long integration times are required.
- We have noticed a slight astigmatism in our images and do not know yet whether it is possible to fully remove it.
- The spatial resolution is seeing-limited to about 1 arcsec.

We plan to fully test our new system for stability and gain more experience doing observations in several wavelength regions. Also, the thickness maps of our etalons will be measured to be able to isolate the cause for the rather broad transmission profiles. To improve the sensitivity in the blue we will use our third generation of ZIMPOL cameras, the ZIMPOL 3, with a backside illuminated sensor. We estimate a gain of light by a factor of 2 for the red and a factor of 4 for the blue. We plan to optimize the optical design and some components and expect another factor of two of more light. The calibration can be performed faster when the FP etalons will be installed on motorized sliders and the routines fully automated. Currently, the FP have to be taken out of the beam and inserted again manually. We expect a duration of the calibration of less than 10 minutes per line. In the summer we plan to start with scientific observations aiming for spatial variations of the Hanle effect in several chromospheric lines.

ACKNOWLEDGMENTS

This work has been funded by the Swiss Nationalfonds, grant no. 200020-117821/1.

REFERENCES

[1] Ramsay, J. V., Kobler, H., and Mugridge, E. G. V., "A new tunable filter with a very narrow pass-band," *Sol. Phys.* **12**, 492–501 (1970).

[2] Cavallini, F., "IBIS: A new post-focus instrument for solar imaging spectroscopy," *Sol. Phys.* **236**, 415–439 (2006).

[3] Kentischer, T. J., Schmidt, W., Sigwarth, M., and Uexkuell, M. V., "TESOS, a double Fabry-Perot instrument for solar spectroscopy," *Astron. Astrophys.* **340**, 569–578 (1998).

[4] Bonaccini, D., Cavallini, F., Ceppatelli, G., and Righini, A., "High resolution solar bidimensional spectroscopy with a Universal Birefringent Filter in tandem with a Fabry-Perot interferometer," *Astron. Astrophys.* **217**, 368–374 (1989).

[5] Bonaccini, D. and Stauffer, F., "High resolution solar bidimensional spectroscopy with a Universal Birefringent Filter in tandem with a Fabry-Perot interferometer: tests and experimental results," *Astron. Astrophys.* **229**, 272–278 (1990).

[6] Cavallini, F., Ceppatelli, G., Righini, A., Meco, M., Paloschi, S., and Tantulli, F., "The spectro-interferometer of the Arcetri Solar Tower," *Astron. Astrophys.* **184**, 386–392 (1987).

[7] Stenflo, J. O., Gandorfer, A., Holzreuter, R., Gisler, D., Keller, C. U., and Bianda, M., "Spatial mapping of the Hanle and Zeeman effects on the Sun," *Astron. Astrophys.* **389**, 314–324 (2002).

[8] Almeida, J. S., Pillet, V. M., and Wittmann, A. D., "The instrumental polarization of a Gregory-Coudé telescope," *Sol. Phys.* **134**, 1–13 (1991).

[9] Feller, A. J., *Instrument Systems for Imaging Spectro-Polarimetry*, PhD thesis, Cuvillier Verlag, Göttingen (2008).

[10] Gandorfer, A. M., Povel, H. P., Steiner, P., Aebersold, F., Egger, U., Feller, A., Gisler, D., Hagenbuch, S., and Stenflo, J. O., "Solar polarimetry in the near UV with the Zurich Imaging Polarimeter ZIMPOL II," *Astron. Astrophys.* **422**, 703–708 (2004).

[11] Povel, H. P., Keller, C. U., and Yadigaroglu, I. A., "Two-dimensional polarimeter with a charge-coupled-device image sensor and a piezoelastic modulator.," *Appl. Opt.* **33**, 4254–4260 (1994).

[12] Thalmann, C., *Applications of High-Precision Polarimetry to Extrasolar Planet Search and Solar Physics*, PhD thesis, ETH Zürich (Switzerland) (2008).

[13] Gisler, D., *Instrumentierung für hochpräzise Vektorpolarimetrie in der Astronomie*, PhD thesis, ETH Zürich (Switzerland) (2005).